

GINK: Graph-based Interaction-aware Kinodynamic Planning via Reinforcement Learning for Autonomous Driving

Se-Wook Yoo, Seung-Woo Seo

Abstract—There are many challenges in applying deep reinforcement learning (DRL) to autonomous driving in a structured environment such as an urban area. This is because the massive traffic flows moving along the road network change dynamically. It is a key factor to detect changes in the intentions of surrounding vehicles and quickly find a response strategy. In this paper, we suggest a new framework that effectively combines graph-based intention representation learning and reinforcement learning for kinodynamic planning. Specifically, the movement of dynamic agents is expressed as a graph. The spatio-temporal locality of node features is conserved and the features are aggregated by considering the interaction between adjacent nodes. We simultaneously learn motion planner and controller that share the aggregated information via a safe RL framework. We intuitively interpret a given situation with predicted trajectories to generate additional cost signals. The dense cost signals encourage the policy to be safe for dynamic risk. Moreover, by utilizing the data obtained through the direct rollout of learned policy, robust intention inference is achieved for various situations encountered in training. We set up a navigation scenario in which various situations exist by using CARLA, an urban driving simulator. The experiments show the state-of-the-art performance of our approach compared to the existing baselines.

I. INTRODUCTION

MOST of the serious accidents that occur every year are caused by human error, such as late discovery or misjudgment. There is an article [1] on potential effects of autonomous driving to reduce accident rates and morality. Although the rule-based conventional methods [2]–[6] divide the problem using hand-crafted state machine or decision trees, there is a limitation that all situations cannot be prescribed in advance. Recently, numerous variants [7]–[9] of DRL [10] that learn policy with a designed reward function have shown impact on generality and efficiency. Nevertheless, in case of structured environment, there are numerous rules that should not be violated, which intensifies the complexity of the problem. RL aims to maximize the expected cumulative reward, but it does not reflect constraints that should be observed. In particular, simply providing a penalty in the form of a negative reward causes serious potential risk in a safety-critical system such self-driving. For this reason, the method [11] was proposed to approximate the expected long-term cost and use it as a constraint for policy optimization. Although it tends to keep minimum restrictions for static objects, it has limitations due to sparse cost signals for moving objects.

The authors are with the Department of Electrical and Computer Engineering, Seoul National University, Republic of Korea. tpdnr1360@snu.ac.kr, sseo@snu.ac.kr

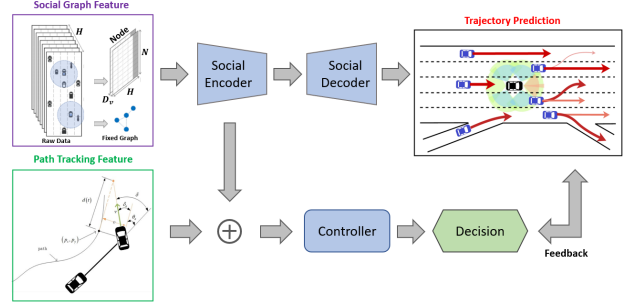


Fig. 1. The proposed scheme. The output of the social encoder is shared for trajectory prediction and decision making. The feedback is exchanged in the form of additional hazard signals or rollout data.

To consider the above issue, we use dense signals generated by geometrically analyzing predicted motions for dynamic agents. Meanwhile, it is particularly difficult to predict trajectories in a congested region. This is because various types of roads (one-way, multi-lane, multi-way intersection, roundabout, etc.) exist and it is more likely to happen occlusion. To solve these, previous works [12]–[14] uses high-definition (HD) map composed of massive data as prior-knowledge, but it is too expensive. In addition, when faced with a dilemma such as illegal parking, the accuracy decrease because of high-dependency on prior-knowledge. To understand the complex interrelationships among traffic participants, [15]–[17] attempted to predict future positions according to perceived maneuvers (change lanes, brake, or keep going, etc.). Unfortunately, incorrect classification of maneuver types has negative results. In order to show robust prediction, [18]–[23] reflects the interaction on social movement as a latent code. In the learned latent code, sequential information about inter-objects is compactly compressed. [18] shows high accuracy through social pooling, but requires high computational cost. In [22], [23], dynamic agents are expressed in graph form to show faster and more accurate results for multi-objects. This is because the spatial significance is considered through the graph convolution network (GCN) [24].

In this paper, we aim to reach the destination along a given route while avoiding the dynamic threat. For efficient and safe driving, the key is to understand the intentions of surrounding vehicles and make appropriate judgments based on the detected risk. Therefore, we present a new framework in Fig. 1 that effectively combines interaction-aware motion planning and control to learn tactical driving strategy. The main idea of the proposed method is to spatio-temporally

refine the intentions of surrounding vehicles using the social encoder, and to simultaneously learn two models that share them through the RL framework. For the social encoder-decoder, the structure of [22] is adopted. We interpret the relationship between the observed objects and the predicted trajectories to generate additional feedback signals and train the controller with them as a constraint. Furthermore, the rollout data that the policy directly executed are used as the ground truth for prediction. The main contributions of the proposed method are as follows.

- Without the need for expensive data, the agent directly interacts with the environment and uses the acquired data to make robust prediction for various situations.
- By interpreting the inferred trajectories and using it as a prediction for risk, constraint policy optimization for dynamic cost is possible.
- It shows that our scheme achieves high performance in many metrics than existing methods in simulations where high traffic and realistic situations exist.

The rest of this paper comprises as follows. The related works are reviewed in Section II. The background is explained in Section III. The proposed scheme and implementation details are described in Section IV. Our experimental results are reported in Section V. Finally, this paper is concluded in Section VI.

II. RELATED WORK

Many works have investigated the methods for collision-free and comfortable self-driving. We address the above problem by combining the two approaches: safe reinforcement learning, interaction-aware motion planning.

A. Safe Reinforcement Learning

In the RL literature, the concept of safety and, conversely, risk is an unavoidable issue in the safety critical domain. Particularly, the constraint Markov decision process (CMDP) [25] to find a solution among the set of allowable policies that guarantee safety is a natural approach. [11] finds a solution by approximating the long-term cost under the CMDP through the policy gradient (PG) algorithm based on Deep RL. To adjust the trade-off caused by the scale difference between reward and cost, [26] propose an alternative penalty in which the designed cost function is multiplied by the learned adaptive weight. Yet, methods of maximizing the average cannot explicitly penalize for rare and fatal situations. Meantime, [27] modifies conditional Value-at-Risk (CVaR) [28] as metric of critic. It minimizes long-tail risk by predicting the full distribution of future returns. [29] derives the PG formula using the CVaR measure to show the behaviors according to the risk-level in a limited scenario.

In contrast, we focus on navigation problems with complex interactions over long periods of time. Furthermore, We adopt a worst-case soft actor critic (WCSAC) [30] method that interprets the CVaR criterion in terms of alternative

penalties. It reduce the potential risk of long-term cost error by balancing between adaptive weights for entropy and safety. Nonetheless, there are several limitations. For example, if a conservative risk-level is used, it is overly pessimistic. Moreover, since most cost signals are sparse, we cannot generalize if small variances pose a large risk. To overcome the aforementioned problems, we combine the interaction-aware motion planning process with the policy optimization method of WCSAC.

B. Interaction-aware Motion Planning

Recently, several studies [31]–[33] have been proposed to integrate RL and planning to learn negotiation skills. They predict the trajectory of surrounding vehicles and then plan the trajectory of the ego vehicle to show reactive behavior, but do not reflect the interaction during planning. Some methods use a predictive model approximated by a partially observable MDP (POMDP) [34] to obtain a tactical driving strategy. For example, in [35], a temporally correlated region is predicted in a search tree created through Monte Carlo tree search (MCTS). Meanwhile, [36] receives temporal sequence of occupancy grid maps (OGMs) for implicit intention reasoning and predicts the time horizon for motion planning. In a different line of work, there have been approaches to encourage cooperative-competitive behavior in a multi-agent system. [37] approximates the sum of the influence of the other agent and its intent as a linear function. [38] uses a GCN-based Q-network that shares the observations of all agents. However, the previous methods require high cost input. Recently, interaction-based prediction methods without requiring expensive resources have been proposed. Some methods using social pooling [18]–[21] showed high accuracy, but are practically intractable for predicting multi-object. Meanwhile, in [39], road context (lane, crosswalk, etc.) and dynamic agents are expressed as vectorized scenes for efficient and intuitive interpretation. Then, it captures high-dimensional global graph relationships that maintain semantic and spatial locality through graph filtering. Similarly, in [22], [23], the surrounding agents are expressed in graph form and accurate and fast prediction results for multi-object are shown. Hence, we adopt the method as a social encoder-decoder structure to maintain spatio-temporal connectivity and reflect interrelationships.

Unlike previous studies, we learn a motion prediction model and a policy that outputs low-level control at the same time, and the two models share a spatio-temporal compressed interaction as an input. In addition, the risk metric is defined through the geometric analysis of predicted motions. By providing rich cost signals generated along an interactive risk metric to the policy optimization process, it creates a meaningful feedback loop between the planner and the decision maker. Eventually, we efficiently estimate the region of attraction that eventually converges to the target state when it stays, and find the optimal policy within that region.

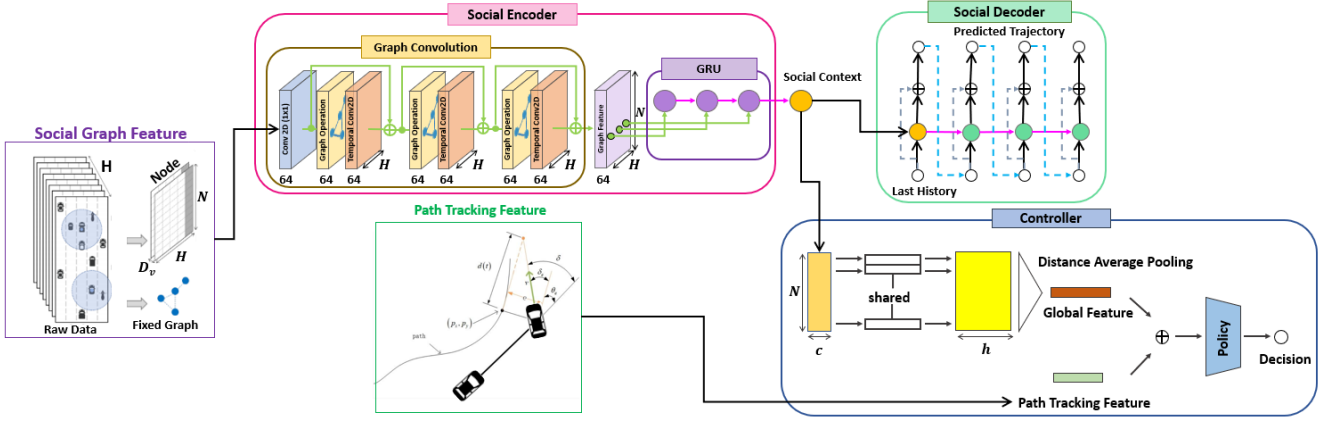


Fig. 2. The overall architecture of our proposed method. Motion planning is performed by social encoder-decoder with social graph features. The controller receives both the feature for following the path and the social context feature that compacts dynamic information. Finally, it outputs interactive behaviors.

III. PRELIMINARIES

A. Constrained Markov Decision Processes (CMDP)

CMDP is an extension of MDP, which is utilized for safe RL. The cost function $\mathcal{C} : \mathcal{S} \times \mathcal{A} \rightarrow \mathbb{R}^+$ is added in a tuple of MDP $(\mathcal{S}, \mathcal{A}, \mathcal{R}, \mathcal{T}, \gamma)$, where \mathcal{S} is a set of states, \mathcal{A} is a set of actions, $\mathcal{R} : \mathcal{S} \times \mathcal{A} \rightarrow \mathbb{R}$ is a reward function, $\mathcal{T} : \mathcal{S} \times \mathcal{A} \times \mathcal{S} \rightarrow [0, 1]$ is a state transition probability distribution, and $\gamma \in (0, 1)$ is a discount factor. The objective of safe RL is to find an optimal policy in a set of allowable policies that satisfy constraints. It maximizes the expected return such that the expected long-term cost remains the below the given threshold d , which is formulated as follows:

$$\mathbb{E}_{\pi} \left[\sum_t \gamma^t r(s_t, a_t) \right] \text{ s.t. } \mathbb{E}_{\pi} \left[\sum_t \gamma^t c(s_t, a_t) \right] \leq d \quad (1)$$

B. Worst-Case SAC (WCSAC)

The limitation of maximizing the average is that it has a high potential risk because of the randomness of the long-term cost. To reduce the long-tail risk, WCSAC algorithm approximates the cost distribution $C_{\pi}(s, a)$ with a Gaussian distribution $\mathcal{N}(Q_{\pi}^c(s, a), V_{\pi}^c(s, a))$, and then replaces the existing measure with a closed-form estimation for CVaR. The risk-sensitive criterion CVaR_{α} for risk-level $\alpha \in (0, 1)$ is computed by:

$$\Gamma_{\pi}^{\alpha}(s, a) \doteq Q_{\pi}^c(s, a) + \alpha^{-1} \phi(\Phi(\alpha)) \sqrt{V_{\pi}^c(s, a)}, \quad (2)$$

where $\phi(\cdot)$ and $\Phi(\cdot)$ are PDF and CDF of standard normal distribution. Furthermore, it encourages the safe exploration by auto-tuning adaptive entropy β and safety weights κ under the problem of maximum entropy RL [40] with safety constraints. For all time t and the given risk-level α , the objective is derived as follows:

$$\mathbb{E}_{\pi} [\beta \log \pi(a_t | s_t) - X_{\alpha, \kappa}^{\pi}(s_t, a_t)] \text{ s.t. } \Gamma_{\pi}^{\alpha}(s_t, a_t) \leq d, \quad (3)$$

where $X_{\alpha, \kappa}^{\pi}(s, a) = Q_{\pi}^r(s, a) - \kappa \Gamma_{\pi}^{\alpha}(s, a)$.

C. Graph Convolution Network (GCN)

As a variant of Convolutional neural network (CNN) [41], GCN reflects flexible adjacency to handle abstract concept like social interaction. It extract valuable information from undirected graph $\mathcal{G} = (\mathcal{V}, \mathcal{E})$. The Node features $v_i \in \mathcal{V} \in \mathbb{R}^{N \times D_v}$ are filtered by aggregating information from adjacent nodes along edges $e_{ij} = (v_i, v_j) \in \mathcal{E}$ with the following propagation rule:

$$\psi(A, H^l; W^l) = \sigma(\tilde{D}^{-\frac{1}{2}} \tilde{A} \tilde{D}^{-\frac{1}{2}} H^l W^l), \quad (4)$$

where an adjacency matrix added self-connections is denoted with $\tilde{A} = A + I_N \in \mathbb{R}^{N \times N}$, a degree matrix with $\tilde{D}_{ii} = \sum_j \tilde{A}_{ij}$, W^l is a layer-specific trainable weight, $\sigma(\cdot)$ denotes an activation function, and $H^l \in \mathbb{R}^{N \times D_h}$ is the embedding vectors in the l^{th} layer; $H^0 = X$.

IV. METHOD

We introduce a framework that efficiently combines intention-aware planning and control to learn strategies to respond to dynamically changed driving styles of surrounding vehicles. Fig. 2 illustrates the detailed structure of each part. It shows how our models interact with environment. The critic and cost model are excluded from the figure because they operate only to evaluate samples extracted from replay buffer. This section describes how the three modules are worked.

A. Input Preprocessing

We use two disentangled input features to perform navigation tasks to the target point. One is a path tracking feature F_k to track the given global path. It explains the kinematics of the system. Another is the social graph features F_d the dynamics of environment to understand the social interaction.

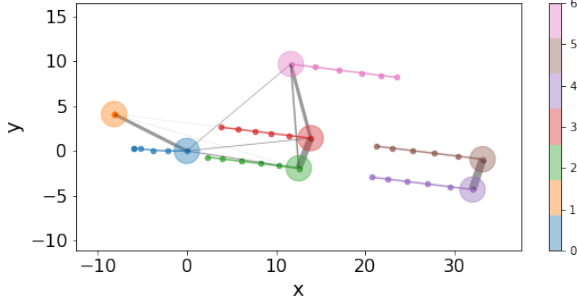


Fig. 3. The visualization of social graph feature. The ego vehicle with index 0 is located at the origin. The inter-frame edges are expressed in the color of each vehicle and show the progress of the movement. The width of gray spatial edge indicates the weight size.

1) *Path Tracking Feature*: The path tracking feature $F_k \in \mathbb{R}^5$ is created by a hybrid method that utilizes both online and offline information. In other words, localization information m_t received through GPS in real-time and road network information \mathcal{G}_n obtained from a database query within a specific area are used. A global path τ_G that follows the road is generated in advance from the present to the target location using the A* algorithm [42]. After that, cross-tracking and heading errors are calculated for the current location and the location before the look-ahead distance by comparing τ_G and m_t . Lastly, the current speed of the ego-vehicle is added.

2) *Social Graph Feature*: We represent the movement of dynamic agents on the road in graph form. F_d consists of the node \mathcal{V} and adjacency matrix \mathbf{A} . It is constructed with manually designed rule as shown in Fig. 3. The node feature is denoted by $\mathcal{V} \in \mathbb{R}^{N \times H \times D_v} = \{v_{it} | i = 1, \dots, N, \text{ and } t = 1, \dots, H\}$, where N is the number of surrounding vehicles, H is the length of history. Each node vector is composed of position and heading angle in the egocentric coordinate system, relative velocity, relative acceleration, relative angular velocity, and mask. The mask means whether the object exists within the recognition area. The edges comprise inter-frame edges $E_F = \{(v_{it}, v_{i(t+1)}) | i = 1, \dots, N, \text{ and } t = 1, \dots, H - 1\}$ and spatial edges $E_S = \{(v_{iH}, v_{jH}) | d_{ij} \leq D_{close} \text{ for } i, j = 1, \dots, N\}$, where d_{ij} is a euclidean distance of two vertices in the last time frame, and D_{close} is the distance threshold for considering neighbors. The adjacency of edges are represented by $A \in \mathbb{R}^{N \times N}$. The elements a_{ij} of A are obtained by indicator function $\mathbb{1}_{\{v_{ie} \in E_S \cup E_F\}}$. To learn high-order relation of interaction, we use $\mathbf{A} \in \mathbb{R}^{L \times N \times N} = \{A_k | k = 1, \dots, L\}$ with multi-hop, where L means the maximum hop. The k^{th} element of \mathbf{A} is as follows:

$$A_k = \{A_k^{ij} = a_{kij} e^{-\frac{d_{ij}}{\tau}} | i, j = 1, \dots, N\}, \quad (5)$$

where a element of A to the k^{th} power is denoted by a_{kij} , and weights of edges are modeled as a Boltzman function with the temperature constant τ .

B. Interaction-aware Planning

Being considered the mutual interplay between ego and other vehicles, trajectories are predicted by seq2seq model. We utilize F_d as inputs without receiving a large amount of information. The structure of the graph is continuously changed over time as agents move or enter/leave the coverage. To enable inductive learning for arbitrary graphs, the planning module is learned using sub-graph samples collected by the RL agent. The module for planning consists of a social encoder ν_η and decoder ρ_ζ .

1) *Social encoder*: In Fig. 2, sub-graphs, which are sampled as much as batch size B from the replay buffer, are used as input for the social encoder. For the B number of sub-graphs, the bottleneck layer, a convolutional layer with a 1 by 1 kernel, is applied to increase the size of node features. After that, the features pass through 3 layers of graph convolutional block to extract higher-order relation representation that encourages sophisticated negotiation strategies. Each graph convolutional block compacts the latent representation over keeping the spatio-temporal local connectivity. Its procedure is as follows. First, similar to Eq.4, the graph operation $\sum_{k=1}^L \psi(A_k, H^l; W_k^l)$ extracts spatially correlated features along edges of graph. Second, a convolution operation is applied along the time axis to understand temporal dependency between dynamic agents, which helps learned intentions to keep consistent. Lastly, a residual connection is utilized to prevent the gradient from being vanished. After multi-layer blocks, to make the social context C , the sequential features are summarized by GRU model.

2) *Social decoder*: Based on the implied intention C , the social decoder generates the future trajectory $\hat{\tau}_t$ of the surrounding vehicle and acts as a teacher to the controller. This is because it can provide signals for long-term risks to the controller by geometrically interpreting the predicted trajectory. The initial hidden state of the decoder GRU is the social context $C \in \mathbb{R}^{N \times c}$ and the initial input is the last location of each vehicle o_t . Each GRU cell predicts the velocity profile of the vehicle through a skip connection between input and output. The prediction module is trained by regression loss with p-norm at each time. The randomly sampled trajectories τ_t from replay buffer are used as the ground truths, which is as follows:

$$\mathcal{L}_P = \mathbb{E}_\pi \left[\frac{1}{H} \sum_{t=1}^H \|\rho_\zeta(\nu_\eta(F_d), o_t) - \tau_t\|_p \right], \quad (6)$$

C. Interaction-aware Control

Our controller module does kinodynamic planning through via RL framework. It uses separate inputs for kinematics and dynamics. We design a pooling module to compress the intentions of vehicles to a lower dimensional space. Moreover, to avoid the long-term risk, an auxiliary costs are generated with the predicted route. This section

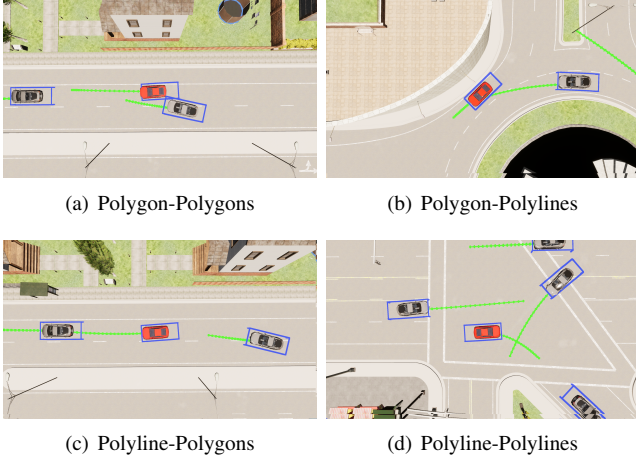


Fig. 4. The 4 cases of social hazard. The color of the ego-vehicle is red and the others are gray. The boundaries with a safety margin are expressed by blue bounding boxes. The green polylines are predicted future trajectories.

explains how to optimize the interaction-aware controller and the planning module at the same time through the off-policy PG method under CMDP.

1) *Distance Average Pooling*: The order of elements along the first axis of social context $C = (c_1, \dots, c_N)$ changes over time. For elements of social context, local features $H_l = (h_1, \dots, h_N) \in \mathbb{R}^{N \times h}$ are obtained through a feed-forward network that shares weights before pooling. In this paper, we propose the distance average pooling (DAP) to create a global feature $H_g \in \mathbb{R}^h$. It maintains the permutation invariant property for the social context containing the intentions of each vehicle. Besides, in terms of the controller of the ego-vehicle, the closer the agents are, the more importantly the intention is reflected. For these reason, we design DAP as follows:

$$H_g = \frac{1}{N} \sum_{i=1}^N h_i \odot e^{-\frac{\sqrt{x_i^2 + y_i^2}}{\tau}}, \quad (7)$$

where τ regulates the influence according to the distance, (x_i, y_i) is the current location of the i^{th} vehicle in egocentric coordinate system, and \odot is defined as the Hadamard-product operation is performed with broadcasting for distance weights. After DAP, we concatenate global feature H_g and hand-designed path tracking feature F_k like $[H_g, F_k]$ and pass them as input to the controller. Each feature explains respectively the dynamics and kinematics of environment.

2) *Auxiliary Cost*: We make the social decoder and controller operate as a teacher-student relationship through the designed feedback. Specifically, it detects the hazard with predicted trajectories by the teacher and provides advice to the student in the form of auxiliary cost for the detected risk. By doing so, it changes the sparse signals to dense ones and promotes the learned controller to avoid long-term risk. We divide the hazard detection into 4 cases as shown in the Fig 4. To interpret the social hazard geometrically, we use

Algorithm 1 GINK

```

1: Initialize: Parameters of networks  $\pi_\theta, Q_\psi, C_\mu, \nu_\eta, \rho_\zeta$ 
2: Initialize: Adaptable weights  $\beta, \kappa$ 
3: Initialize: Replay buffer  $\mathcal{D} \leftarrow \emptyset$ 
4: Copy target networks  $\langle \bar{\theta}, \bar{\psi}, \bar{\mu} \rangle$  with  $\langle \theta, \psi, \mu \rangle$ 
5: Load road network graph  $\mathcal{G}_n$  from database
6: for each iteration do
7:   Randomly select  $p_s$  and  $p_g$ 
8:    $\tau_g \leftarrow A^*(p_s, p_g, \mathcal{G}_n)$ 
9:   for each environmental step do
10:     $F_d \leftarrow \phi_d(o_{t-H+1:t})$  and  $F_k \leftarrow \phi_k(\tau_g, m_t)$ 
11:     $\check{F}_d \leftarrow \phi_d(o_{t-2H+1:t})$  centered on  $t - H$  time.
12:     $C \leftarrow \nu_\eta(F_d)$ 
13:     $s_t = \{C, F_k\}$ 
14:     $a_t \sim \pi_\theta(a_t | s_t)$ 
15:     $s_{t+1} \sim \mathcal{T}(s_{t+1} | s_t, a_t)$ 
16:     $\hat{\tau}_t \leftarrow \rho_\zeta(C, o_t)$ 
17:     $c_t^+ = c(s_t, a_t) + \hat{c}(\hat{\tau}_t)$ 
18:     $\mathcal{D} \leftarrow \mathcal{D} \cup \{s_t, a_t, r(s_t, a_t), c_t^+, s_{t+1}, \check{F}_d\}$ 
19:   end for
20:   for each gradient step do
21:     Randomly sample experience from  $\mathcal{D}$ 
22:     Update  $\eta, \zeta$  with  $\nabla_{\eta, \zeta} \mathcal{L}_p(\check{F}_d)$  from Eq. 6
23:      $\theta, \psi, \mu, \beta, \kappa \leftarrow \text{WCSAC}(s_t, a_t, r_t, c_t^+, s_{t+1})$ 
24:     Update  $\langle \bar{\theta}, \bar{\psi}, \bar{\mu} \rangle$  with  $\langle \theta, \psi, \mu \rangle$ 
25:   end for
26: end for

```

polygons and polylines. Polygon is a local bounding box with safety margin (ϵ_l, ϵ_w) added to the length and width of each vehicle. The polyline means the trajectory of each vehicle predicted by ρ_ζ . For the case of Fig. 4(a), we check for overlapping between polygon of ego-vehicle and others through separating axis theorem (SAT) [43]. In the cases of Fig. 4(b-d), we utilize a method [44] to check intersection between two line segments based on a counter-clockwise (CCW) algorithm. We connect the starting and ending points of polygons to make line segments. For the bounding box, we use each side as a line segment. The predicted auxiliary cost is defined as follows:

$$\hat{c}_\rho = \mathbb{1}_{\{\mathbf{G} \cap \mathbf{G}\}} \vee \mathbb{1}_{\{\mathbf{G} \cap \mathbf{L}\}} \vee \mathbb{1}_{\{\mathbf{L} \cap \mathbf{G}\}} \vee \mathbb{1}_{\{\mathbf{L} \cap \mathbf{L}\}}, \quad (8)$$

where G and L are polygon and polyline of ego-vehicle respectively. The bold font means set of others. \cap represents a set of intersection between ego-ones and others, and \vee is a OR operator.

3) *Optimization*: In this section, Graph-based INTention-aware Kinodynamic planning method, namely GINK, is briefly described in Alg. 1. Before going to a new episode, we obtain global path τ_g that follows road network \mathcal{G}_n with A* algorithm (lines 7-8). At each environmental step, the agent interacts with environment and generates samples for training and stores them in a buffer (lines 9-19). Input pre-processing modules are ϕ_d and ϕ_k . They operate separately

TABLE I
COMPARISON AVERAGE RESULTS WITH STANDARD DEVIATION IN NAVIGATION SCENARIO

METHOD	RETURN	SUCCESS RATE	DISTANCE	COST	COLLISION RATE	STEP	SUCCESS STEP
SAC	944.50 \pm 597.69	0.48 \pm 0.07	122.18 \pm 73.17	11.53 \pm 16.63	0.44 \pm 0.06	253.90 \pm 148.35	366.01 \pm 74.96
WCSAC	984.37 \pm 557.17	0.54 \pm 0.11	129.88 \pm 70.84	7.16 \pm 13.08	0.35 \pm 0.12	325.26 \pm 178.76	432.05 \pm 85.48
GINK (Ours)	1283.49 \pm 487.64	0.76 \pm 0.03	161.19 \pm 57.76	4.03 \pm 10.39	0.19 \pm 0.03	302.61 \pm 119.13	337.34 \pm 69.48

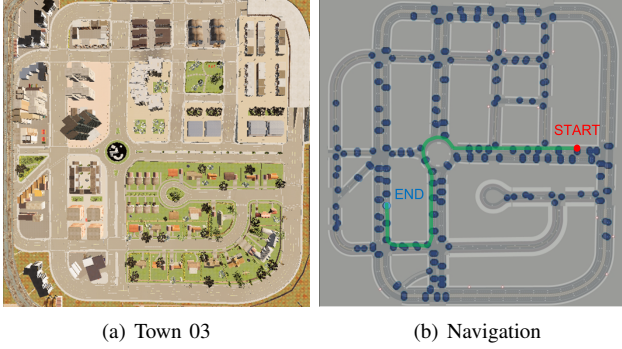


Fig. 5. The visualization of the navigation environment. (a) is the map used in the virtual environment and (b) explains an episode. All possible spawn points are represented by navy dots. In addition, the start and end are red and blue respectively. The route of navigation is drawn in green.

to make social graph feature F_d or path tracking feature F_k (line 10). In fact, F_d is to grasp the dynamics of environment from the history of observations and F_k is to understand the kinematics of system. Additionally, we accumulate another feature \tilde{F}_d centered at the midpoint of length $2H$ to use as ground truth for future trajectories $\hat{\tau}_t$ (line 11). Given state processed by social encoder ν_η , agent execute a action and then proceeds to the next state (lines 12-15). In order to avoid the long-term risk considering the interaction, we use auxiliary cost in Eq. 8. It is designed by using $\hat{\tau}_t$ predicted by social decoder ρ_ζ (lines 16-18). For the gradient step, all parameters of models are updated with batches sampled from \mathcal{D} (lines 20-25). The social encoder and decoder are updated by prediction loss in Eq. 6. The actor, critic, approximated cost and adaptable weights are learned by WCSAC algorithm with accumulated samples to solve objective in Eq. 3. Lastly, the parameters of target networks are updated by moving averages to increase learning stability.

V. EXPERIMENTS

A. Simulation Settings

To demonstrate performance in the safety and effectiveness of the proposed method, as shown Fig. 5, we set a navigation environment that contains diverse scenes by utilizing the CARLA physics engine. The process of navigation is composed of various types of driving scenes interacting between dynamic agents. In order to include the real-like natural distribution in the virtual environment, the following situation is assumed. Start and end points with a fixed route length are randomly selected, traffic lights and traffic signs are ignored, and the speed difference percentage of each vehicle is 20 percent. To track referenced path obtained by the A^* algorithm, a reward function is designed as follows:

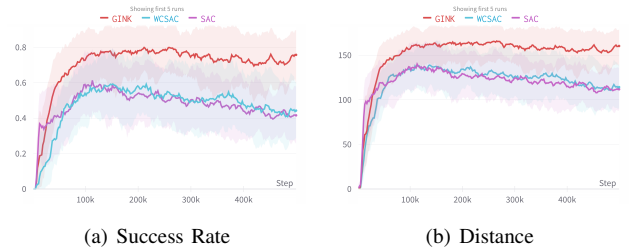


Fig. 6. Learning curve for navigation environment. The darker-colored lines and shaded areas denote the average return and standard deviations.

$$w_1|v_s| + w_2|v_d| + w_3|e_c| + w_4|\Delta e_c| + w_5|\delta_s| + w_6|e_h||v_d|, \quad (9)$$

where v_s and v_d are longitudinal and latitudinal velocities over the reference path, e_c and e_h are cross tracking and heading angle errors, and δ_s is a steering wheel angle, and lastly (w_1, \dots, w_6) are the experimentally obtained weights. To avoid a collision, the environmental cost function is calculated with normalized collision intensity.

B. Metrics

We set the following 7 measurements to compare how much the driving strategies are tactical: return, success rate, distance, cost, collision rate, step, and success step. The return, distance, cost, and step mean total cumulative rewards, distances, costs, and steps that are given during an episode. The success rate is the rate of episodes that the destination is reached. The collision rate is the rate of episodes that which there are crashes. Finally, the success step means the total number of steps over successful episodes. On a different side, to compare how behaviors are accurately predicted, we used average displacement error (ADE) and final displacement error (FDE). All of above metrics are measured by the averages of 5 seeds over 100 episodes.

C. Tactical Driving Strategy

We evaluated performance of models in terms of efficiency and safety according to various metrics. As in our method, SAC and WCSAC algorithms based on off-policy maximum entropy RL framework are adopted as baselines. In order for fair comparison, the baselines also use separate features for kinematics and dynamics as inputs. The difference is that they employ observations at a single time frame as the dynamic feature. After that, the max pooling is applied to obtain global feature. Table. I represents the averages with standard deviations for each method with regard to efficiency

TABLE II
COMPARISON TRAJECTORY PREDICTION RESULTS

METHOD	ADE	FDE
V-GRU	0.57 ± 0.10	1.45 ± 0.26
GRIP	0.55 ± 0.07	1.32 ± 0.20
GINK (Ours)	0.48 ± 0.06	1.15 ± 0.19

and safety metrics. WCSAC has slightly better performance and smaller standard deviation than SAC. Since using the worst case measurement to reduce potential risk, it reduces the probability of collision as shown in cost and collision rate and also increases the survival time as shown in step. Nevertheless, it still has limitations. Because it does not capture dynamic costs, it still has a high percentage of crash situations. This is because the long-term dynamic risk tends not to be reflected as the cost signal is sparsely given only when a crash occurs. Furthermore, a large increase in the success step means that it is a loss in terms of efficiency by driving conservatively.

On the other hand, our method shows a dramatic improvement in all respects: 30.4% in return, 40.7% in success rate, 24.1% in distance, 77.7% in cost, 84.2% in collision rate, and 8.5% in success step. Although the survival time of the episode was increased compared to WCSAC in the step, it is an effect due to an efficient driving strategy in view of a large decrease in the success step. Moreover, unlike baselines that show similar curves, our method shows a significant improvement in sampling efficiency and stability through the Fig. 6. Although SAC has a faster initial learning speed due to more aggressive driving than WCSAC, collisions occur frequently and eventually converge to a lower value. As a result, the convergence performance gradually decreases. In contrast, our method shows stable convergence at high values. The reason is that social encoders capture features between objects with local connectivity taken into account through graph operation and aggregate motion patterns through temporal convolution. It also utilizes dense long-term cost signals for policy optimization by interpreting predicted behaviors through social decoders.

D. Robust Behavior Prediction

In this section, we evaluate the performance of motion prediction for models with a sequence-to-sequence structure using metrics such as ADE and FDE. We adopt vanilla gated recurrent unit (V-GRU) and graph-based interaction-aware trajectory prediction (GRIP) algorithms as the baselines.

TABLE III
EFFECT OF INTERACTION-AWARE PLANING

METHOD	SUCCESS RATE	COLLISION RATE	SUCCESS STEP
RN + WCSAC	0.34 ± 0.05	0.33 ± 0.05	418.11 ± 50.0
HMM + WCSAC	0.22 ± 0.05	0.25 ± 0.05	599.35 ± 50.0
V-GRU + WCSAC	0.11 ± 0.08	0.19 ± 0.09	482.55 ± 127.22
SE + WCSAC	0.71 ± 0.03	0.20 ± 0.02	360.46 ± 31.52

TABLE IV
CHANGES IN PERFORMANCE WHILE ADJUSTING THE MODEL

INDEX	COST	WEDGE	DAP	AUX. COST	SUCCESS RATE
B1	N	N	N	N	0.33 ± 0.12
B2	N	Y	N	N	0.42 ± 0.10
B3	N	Y	Y	N	0.67 ± 0.14
B4	Y	N	N	N	0.45 ± 0.05
B5	Y	N	Y	N	0.69 ± 0.10
B6	Y	Y	Y	N	0.71 ± 0.09
B7 (GINK)	Y	Y	Y	Y	0.76 ± 0.03

Specifically, GRIP excludes the controller part that is learned with the RL framework in our method. In the case of V-GRU, the graph convolution part is excluded from the social encoder in GRIP. The difference between GRIP and V-GRU is whether or not it reflects regional interrelationships in the spatial domain. In both baseline cases, 200 episodes successfully performed by the autopilot agent provided by CARLA is used for training data. In order to compare the generalizability of various scenes, 20 episodes including both successes and failures are collected for test data.

GRIP reduces errors slightly in ADE than V-GRU, but definitely reduces errors a lot in FDE. It makes sense in that most vehicles interact longitudinally along the lane. In contrast to GRIP, our method shows a greater improvement and stability in both compared to baselines: 14.6% in ADE and 14.8% in FDE. It is noteworthy that this performance is achieved even without pre-prepared training data. This is because it has the advantage of being able to utilize the data of various scenes obtained in the trial and error process of reinforcement learning. In this paper, the existing graph-based methods overcome the difficulties of dynamic graph generalization through combination with RL.

E. Ablation Study

To prove the effect of recognizing interactions by reflecting the topological characteristics of surrounding objects, we construct the following experiment. For a fair comparison, Eq. 6 to train social decoders is excluded from the objective function. Although models of the social encoder are modified, all policies are equivalently optimized by WCSAC algorithm in Eq. 3. To be specific, social context from random noise (RN) is sampled from standard normal distribution. A hidden Markov model (HMM) is pretrained with 500 samples of accident-free scenes obtained via autopilot agent. In order to apply it to continuous observation, the emission probability is modeled as a Gaussian variable. Moreover, the social context is approximated with a categorical variable with 3 levels. Incidentally, V-GRU means that the graph convolution module is excluded from the social encoder. As shown in Table. III, a method that uses social encoder (SE) shows a dramatic improvement over others. The reason is that the spatio-temporally abstracted features express effectively the dynamic interaction for tactical driving. On the other hand, it has better results when using random noise than others. For the V-GRU, this is because the intent of distant objects rather interferes with the perception of surrounding

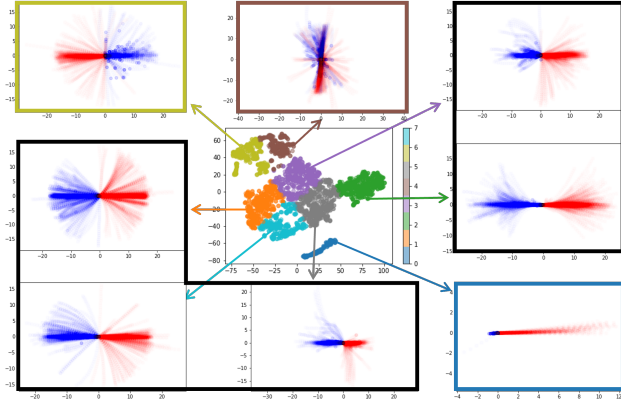


Fig. 7. Visualization of social context with trajectory distributions. The color to distinguish the social context means the label for each trajectory distribution. In the trajectory distribution, the blue part is the previous history and the red part is the predicted future.

circumstances, which can have fatal consequences. Furthermore, in the case of HMM, it cannot adapt to the environment in which collision exists. This is because it was only trained in a collision-free environment.

Table. IV shows how much each module contributes to the performance improvement. By comparing B1-B3 and B4-B7, the impact of modifying each module is evaluated depending on whether or not cost is used as a constraint of policy optimization. Difference from B1 to B2 and from B5 to B6 represents the degree of improvement by using weighted edge (Wedge) through the Eq. 5. Compared to B2, B3 and B4, B5, distance average pooling (DAP) in Eq. 7 makes big improvement due to the fact that it helps a lot with ego-centered control by paying attention to spatially nearby objects. Lastly, B7 verifies that auxiliary cost (Aux. Cost) increases the performance because dense signals make planning longer on the side of safety.

F. Visualization

To illustrate the meaning of the learned social context vectors, we cluster the distribution of that by using the t-distributed stochastic neighbor embedding (TSNE) method. Trajectory distribution for each cluster is shown in Fig. 7. It can be seen that the semantical meaning is divided according to the direction and shape of the distribution. Specifically, the 6th cluster (yellow) is a distribution that moves in the opposite direction to the ego-vehicle, the 4th distribution (brown) moves in the vertical direction to the ego-vehicle, and the 0th one (blue) refers to the intention to stand still and move forward. The other distribution sets (black) are all in the same direction, but with slightly different velocities and shapes. This makes sense in that most of the patterns encountered are in the same direction and the latent vectors are in a similar location.

VI. CONCLUSION

In this work, we propose an approach that combines graph-based interaction-aware planning with DRL to track a

path while avoiding a collision. The main idea is to learn a social context vector that summarizes the sequence of observations by alternately passing through multi-layer graph operation and temporal convolution. Furthermore, it enables long-term planning by using the dense cost signal created by geometrically analyzing the relationship between predicted paths as a constraint for policy optimization. It makes a significant performance improvement in navigation problems with dense traffic, which was limited in existing baselines. Then, it interprets the learned variables and visualizes them to show meaningful results.

In the future, we will extend our work on how to consider multi-modal trajectory distribution or reflect more road context information in graph form. Another exciting direction would be to investigate the kinodynamic planning methods that require to learn path-following features while avoiding uncertain obstacles in a wild environment.

ACKNOWLEDGMENT

This work was supported by the Basic Science Research Program through the National Research Foundation of Korea (NRF) funded by the Ministry of Science and ICT(2017R1E1A1A01075171) and in part by the Institute of New Media and Communications and the Automation and Systems Research Institute, Seoul National University.

REFERENCES

- [1] D. Milakis, B. Van Arem, and B. Van Wee, "Policy and society related implications of automated driving: A review of literature and directions for future research," *Journal of Intelligent Transportation Systems*, vol. 21, no. 4, pp. 324–348, 2017.
- [2] A. Barbera, J. Horst, C. Schlenoff, E. Wallace, and D. Aha, "Developing world model data specifications as metrics for sensory processing for on-road driving tasks," tech. rep., NATIONAL INST OF STANDARDS AND TECHNOLOGY GAITHERSBURG MD, 2003.
- [3] A. J. Barbera, J. A. Horst, C. I. Schlenoff, and D. W. Aha, "Task analysis of autonomous on-road driving," in *Mobile Robots XVII*, vol. 5609, pp. 61–72, International Society for Optics and Photonics, 2004.
- [4] C. Urmson, J. Anhalt, D. Bagnell, C. Baker, R. Bittner, M. Clark, J. Dolan, D. Duggins, T. Galatali, C. Geyer, et al., "Autonomous driving in urban environments: Boss and the urban challenge," *Journal of field Robotics*, vol. 25, no. 8, pp. 425–466, 2008.
- [5] M. Montemerlo, J. Becker, S. Bhat, H. Dahlkamp, D. Dolgov, S. Ettinger, D. Haehnel, T. Hilden, G. Hoffmann, B. Huhne, et al., "Junior: The Stanford entry in the urban challenge," *Journal of field Robotics*, vol. 25, no. 9, pp. 569–597, 2008.
- [6] M. Olsson, "Behavior trees for decision-making in autonomous driving," 2016.
- [7] S. Shalev-Shwartz, S. Shammah, and A. Shashua, "Safe, multi-agent, reinforcement learning for autonomous driving," *arXiv preprint arXiv:1610.03295*, 2016.
- [8] A. E. Sallab, M. Abdou, E. Perot, and S. Yogamani, "Deep reinforcement learning framework for autonomous driving," *Electronic Imaging*, vol. 2017, no. 19, pp. 70–76, 2017.
- [9] S. Wang, D. Jia, and X. Weng, "Deep reinforcement learning for autonomous driving," *arXiv preprint arXiv:1811.11329*, 2018.
- [10] R. S. Sutton, A. G. Barto, et al., *Introduction to reinforcement learning*, vol. 135. MIT press Cambridge, 1998.
- [11] J. Achiam, D. Held, A. Tamar, and P. Abbeel, "Constrained policy optimization," in *International conference on machine learning*, pp. 22–31, PMLR, 2017.
- [12] A. Houenou, P. Bonnifait, V. Cherfaoui, and W. Yao, "Vehicle trajectory prediction based on motion model and maneuver recognition," in *2013 IEEE/RSJ international conference on intelligent robots and systems*, pp. 4363–4369, IEEE, 2013.

- [13] V. Karasev, A. Ayvaci, B. Heisele, and S. Soatto, "Intent-aware long-term prediction of pedestrian motion," in *2016 IEEE International Conference on Robotics and Automation (ICRA)*, pp. 2543–2549, IEEE, 2016.
- [14] Y. Yoon, T. Kim, H. Lee, and J. Park, "Road-aware trajectory prediction for autonomous driving on highways," *Sensors*, vol. 20, no. 17, p. 4703, 2020.
- [15] M. Schreier, V. Willert, and J. Adamy, "Bayesian, maneuver-based, long-term trajectory prediction and criticality assessment for driver assistance systems," in *17th international ieee conference on intelligent transportation systems (ITSC)*, pp. 334–341, IEEE, 2014.
- [16] Q. Tran and J. Firl, "Online maneuver recognition and multimodal trajectory prediction for intersection assistance using non-parametric regression," in *2014 IEEE intelligent vehicles symposium proceedings*, pp. 918–923, IEEE, 2014.
- [17] J. Schlechtriemen, F. Wirthmueller, A. Wedel, G. Breuel, and K.-D. Kuhnert, "When will it change the lane? a probabilistic regression approach for rarely occurring events," in *2015 IEEE Intelligent Vehicles Symposium (IV)*, pp. 1373–1379, IEEE, 2015.
- [18] N. Deo and M. M. Trivedi, "Convolutional social pooling for vehicle trajectory prediction," in *Proceedings of the IEEE Conference on Computer Vision and Pattern Recognition Workshops*, pp. 1468–1476, 2018.
- [19] A. Alahi, K. Goel, V. Ramanathan, A. Robicquet, L. Fei-Fei, and S. Savarese, "Social lstm: Human trajectory prediction in crowded spaces," in *Proceedings of the IEEE conference on computer vision and pattern recognition*, pp. 961–971, 2016.
- [20] A. Gupta, J. Johnson, L. Fei-Fei, S. Savarese, and A. Alahi, "Social gan: Socially acceptable trajectories with generative adversarial networks," in *Proceedings of the IEEE conference on computer vision and pattern recognition*, pp. 2255–2264, 2018.
- [21] A. Vemula, K. Muelling, and J. Oh, "Social attention: Modeling attention in human crowds," in *2018 IEEE international Conference on Robotics and Automation (ICRA)*, pp. 4601–4607, IEEE, 2018.
- [22] X. Li, X. Ying, and M. C. Chuah, "Grip: Graph-based interaction-aware trajectory prediction," in *2019 IEEE Intelligent Transportation Systems Conference (ITSC)*, pp. 3960–3966, IEEE, 2019.
- [23] X. Li, X. Ying, and M. C. Chuah, "Grip++: Enhanced graph-based interaction-aware trajectory prediction for autonomous driving," *arXiv preprint arXiv:1907.07792*, 2019.
- [24] T. N. Kipf and M. Welling, "Semi-supervised classification with graph convolutional networks," *arXiv preprint arXiv:1609.02907*, 2016.
- [25] E. Altman, *Constrained Markov decision processes: stochastic modeling*. Routledge, 1999.
- [26] C. Tessler, D. J. Mankowitz, and S. Mannor, "Reward constrained policy optimization," *arXiv preprint arXiv:1805.11074*, 2018.
- [27] Y. Chow, M. Ghavamzadeh, L. Janson, and M. Pavone, "Risk-constrained reinforcement learning with percentile risk criteria," *The Journal of Machine Learning Research*, vol. 18, no. 1, pp. 6070–6120, 2017.
- [28] R. T. Rockafellar, S. Uryasev, *et al.*, "Optimization of conditional value-at-risk," *Journal of risk*, vol. 2, pp. 21–42, 2000.
- [29] Y. C. Tang, J. Zhang, and R. Salakhutdinov, "Worst cases policy gradients," *arXiv preprint arXiv:1911.03618*, 2019.
- [30] Q. Yang, T. D. Simão, S. H. Tindemans, and M. T. Spaan, "Wcsac: Worst-case soft actor critic for safety-constrained reinforcement learning," in *Proceedings of the Thirty-Fifth AAAI Conference on Artificial Intelligence*. AAAI Press, online, 2021.
- [31] M. Werling, J. Ziegler, S. Kammel, and S. Thrun, "Optimal trajectory generation for dynamic street scenarios in a frenet frame," in *2010 IEEE International Conference on Robotics and Automation*, pp. 987–993, IEEE, 2010.
- [32] P. Nilsson, L. Laine, N. Van Duijkeren, and B. Jacobson, "Automated highway lane changes of long vehicle combinations: A specific comparison between driver model based control and non-linear model predictive control," in *2015 International Symposium on Innovations in Intelligent Systems and Applications (INISTA)*, pp. 1–8, IEEE, 2015.
- [33] F. Damerow and J. Eggert, "Risk-averse behavior planning under multiple situations with uncertainty," in *2015 IEEE 18th International Conference on Intelligent Transportation Systems*, pp. 656–663, IEEE, 2015.
- [34] M. J. Kochenderfer, *Decision making under uncertainty: theory and application*. MIT press, 2015.
- [35] C.-J. Hoel, K. Driggs-Campbell, K. Wolff, L. Laine, and M. J. Kochenderfer, "Combining planning and deep reinforcement learning in tactical decision making for autonomous driving," *IEEE transactions on intelligent vehicles*, vol. 5, no. 2, pp. 294–305, 2019.
- [36] Z. Wang, Y. Zhuang, Q. Gu, D. Chen, H. Zhang, and W. Liu, "Reinforcement learning based negotiation-aware motion planning of autonomous vehicles," in *2021 IEEE/RSJ International Conference on Intelligent Robots and Systems (IROS)*, pp. 4532–4537, IEEE, 2021.
- [37] S. Qi and S.-C. Zhu, "Intent-aware multi-agent reinforcement learning," in *2018 IEEE International Conference on Robotics and Automation (ICRA)*, pp. 7533–7540, IEEE, 2018.
- [38] J. Jiang, C. Dun, T. Huang, and Z. Lu, "Graph convolutional reinforcement learning," *arXiv preprint arXiv:1810.09202*, 2018.
- [39] J. Gao, C. Sun, H. Zhao, Y. Shen, D. Anguelov, C. Li, and C. Schmid, "Vectornet: Encoding hd maps and agent dynamics from vectorized representation," in *Proceedings of the IEEE/CVF Conference on Computer Vision and Pattern Recognition*, pp. 11525–11533, 2020.
- [40] T. Haarnoja, H. Tang, P. Abbeel, and S. Levine, "Reinforcement learning with deep energy-based policies," in *International Conference on Machine Learning*, pp. 1352–1361, PMLR, 2017.
- [41] A. Krizhevsky, I. Sutskever, and G. E. Hinton, "Imagenet classification with deep convolutional neural networks," in *Advances in Neural Information Processing Systems* (F. Pereira, C. J. C. Burges, L. Bottou, and K. Q. Weinberger, eds.), vol. 25, Curran Associates, Inc., 2012.
- [42] D. Keirsey, E. Koch, J. McKisson, A. Meystel, and J. Mitchell, "Algorithm of navigation for a mobile robot," in *Proceedings. 1984 IEEE International Conference on Robotics and Automation*, vol. 1, pp. 574–583, IEEE, 1984.
- [43] J. Huynh, "Separating axis theorem for oriented bounding boxes," URL: jkh.me/files/tutorials/Separating%20Axis%20Theorem%20for%20Oriented%20Bounding%20Boxes.pdf, 2009.
- [44] B. Chazelle and H. Edelsbrunner, "An optimal algorithm for intersecting line segments in the plane," *Journal of the ACM (JACM)*, vol. 39, no. 1, pp. 1–54, 1992.